

Extension and customization of self-stability control in compliant legged systems

M Ernst¹, H Geyer² and R Blickhan¹

¹ Science of Motion, Institute of Sport Science, Friedrich-Schiller University, Seidelstrasse 20, 07749 Jena, Germany

² Robotics Institute, Carnegie Mellon University, Pittsburgh, PA 15213, USA

E-mail: michael.ernst@uni-jena.de, hgeyer@cs.cmu.edu and reinhard.blickhan@uni-jena.de

Received 4 September 2011

Accepted for publication 20 June 2012

Published 13 July 2012

Online at stacks.iop.org/BB/7/046002

Abstract

Several recent studies on the control of legged locomotion in animal and robot running focus on the influence of different leg parameters on gait stability. In a preceding investigation self-stability controls showing deadbeat behavior could be obtained by studying the dynamics of the system in dependence of the leg orientation carefully adjusted during the flight phase. Such controls allow to accommodate disturbances of the ground level without having to detect them. Here we further this method in two ways. Besides the leg orientation, we allow changes in leg stiffness during flight and show that this extension substantially improves the rejection of ground disturbances. In a human like example the tolerance of random variation in ground level over many steps increased from 3.5% to 35% of leg length. In single steps changes of about 70% leg length (either up or down) could be negotiated. The variable leg stiffness not only allows to start with flat leg orientations maximizing step tolerances but also increase the control subspace. This allows to customize self-stability controls and to consider physical and technical limitations found in animals and robots.

1. Introduction

Many legged animals and robots use compliant leg behavior in stance (McMahon 1985, Raibert 1986, Alexander 1990, Papadopoulos and Buehler 2000, Altendorfer *et al* 2001, Hosoda *et al* 2008, Radkhah *et al* 2010, Park *et al* 2011). For these systems, the spring-mass model (Blickhan 1989, McMahon and Cheng 1990) has evolved into a standard template to study locomotion control (Full and Koditschek 1999). While early work focused on using the spring-mass model in the development of feedback controllers for hopping and running machines (Raibert 1986), more recent studies emphasize its use in identifying feedforward controls that take advantage of this model's self-stability in running.

Self-stability in running has first been demonstrated by Ringrose (1997) who showed that, like passive dynamic walkers (McGeer 1990a, 1990b, Collins *et al* 2005), running robots require no feedback about the ground level to enter and maintain steady-state locomotion. This observation has

been confirmed in theoretical studies. Investigating cockroach running, Schmitt and Holmes (2000a, 2000b) and Seipel *et al* (2004) identified parameters of the spring-mass model that produce self-stable locomotion in the horizontal plane. Likewise, Seyfarth *et al* (2002) demonstrated self-stability for running in the sagittal plane. In addition, they found that human runners seem to explore this self-stable behavior as they choose leg parameters required for it. More recent studies have analyzed the influence of several flight and stance phase model parameters on self-stability, including the stiffness, orientation and length of the leg in flight (Blum *et al* 2007, 2010, Ernst *et al* 2009), and the leg rest length and nonlinear leg stiffness behavior in stance (Owaki and Ishiguro 2006, Rummel and Seyfarth 2008, Schmitt and Clark 2009, Karssen and Wisse 2011).

In general, however, these studies first propose particular control strategies (in parameter space) and then investigate their influence on self-stability (Seyfarth *et al* 2002, Geyer *et al* 2006, Owaki and Ishiguro 2006, Schmitt 2006, Seipel

and Holmes 2007, Rummel and Seyfarth 2008, Ankarali and Saranli 2010, Blum *et al* 2007, 2010). The reverse approach, we followed up in this study, of deriving controls from carefully studying parameter influences on self-stability is seldom pursued, although it promises a more complete understanding of the theoretical potential and limits of self-stability control. For example, Sugimoto and Osuka (2005) and Owaki *et al* (2009) captured the underlying stabilization mechanism of passive dynamic walking and running with an approximate linearized Poincaré map which they reformulated as a negative feedback system. This reformulation allowed the authors to identify explicit model parameter combinations as feedback gains which guarantee self-stability if they are smaller than one. In another example, Seyfarth and Geyer (2002) studied how the leg orientation in swing manipulates the resulting Poincaré map of the spring mass model in running and derived a deadbeat control that guarantees running stability for comparably large disturbances in the ground level. Recently, Ankarali and Saranli (2010) extended the deadbeat control to also compensate for damping losses during stance.

Although the manipulation of the Poincaré map by parameter adaptations has been shown to yield controllers that largely increase the robustness and stability of spring-mass running (Seyfarth and Geyer 2002), this method has not been explored to its full potential. In the previous studies only one parameter, the swing leg angle, has been considered for the manipulation, and the extent to which gait stability and robustness can be improved by including other model parameters remains unclear.

Here we further this method in two ways. First, we include the spring stiffness and the system energy as two important parameters in the Poincaré map manipulation and show that they largely extend the theoretical limit of self-stability and robustness with respect to ground disturbances and locomotion speed. In addition we demonstrate how physical and technical limitations found in animals and robots can be taken into account in a rigorous way to customize self-stability control for individual legged systems, maximizing their use of self-stability control.

2. Self-stability control

The spring-mass model (figure 1) reduces the body to a point mass that moves on a ballistic trajectory in flight and rebounds on a massless spring leg (stiffness k , rest length ℓ_0) in stance. The transition between stance and flight is defined by the spring leg extending to ℓ_0 during rebound, and the transition between flight and stance is given by a landing condition

$$y_\ell = \ell_0 \sin(\alpha), \quad (1)$$

where α is the leg orientation during flight with respect to gravity (gravitational acceleration $g = 9.81 \text{ m s}^{-2}$; figure 1). Because of this landing condition, for a fixed system energy E_{sys} , periodic locomotion and its stability can be investigated by mapping only one variable, the apex height y_i , from one apex, i , to the next, $i + 1$ (Seyfarth *et al* 2002). In the picture of the apex return map, running is periodic if $y_{i+1} = y_i = y^*$, where y^* is the steady state solution, and stable if $|\partial y_{i+1} / \partial y_i| < 1$ within a neighborhood of y^* .

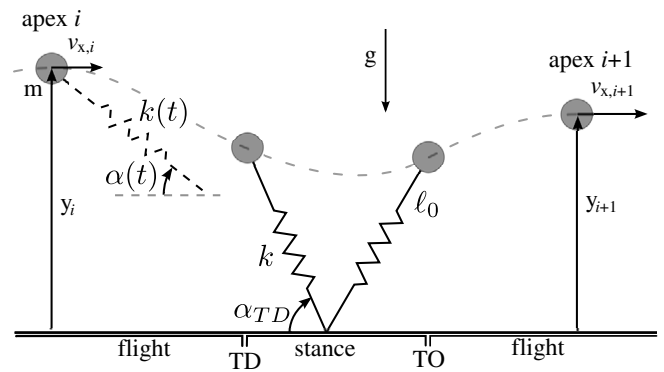


Figure 1. Spring-mass model. The model consists of a point mass m , which in stance rebounds on a massless spring with stiffness k and rest length ℓ_0 . TD with angle α_{TD} occurs when the model hits the ground. The model takes off when the spring relaxes to ℓ_0 in stance (TO). The pairs $(y, v_x)_i$ and $(y, v_x)_{i+1}$ denote the system state at two consecutive apices. $\alpha(t)$ and $k(t)$ describe control strategies executed from apex to TD. g : gravitational acceleration ($g = 9.81 \text{ m s}^{-1}$).

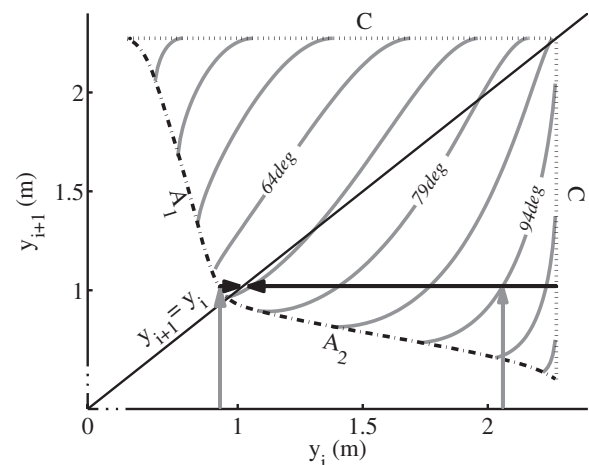


Figure 2. Example return map. The return map $y_{i+1}(y_i)$ is shown for different TD leg orientations α_{TD} . Black arrows indicate a deadbeat return map which projects different start heights y_i (gray arrows) into a desired apex height $y_{\text{des}} = 1 \text{ m}$ within one step. A_1 , A_2 and C describe the limits of the return map. A_1 indicates where y_i is below the landing height (compare (1), figure 3(A)). At A_2 , the model stumbles after take off ($y(t_{TO}) > y(t > t_{TO})$, figure 3(D)). At C , the potential energy $E_{\text{pot}} = y_i mg$ equals the system energy E_{sys} . Parameters: $k = 30 \text{ kN m}^{-1}$, $\ell_0 = 1 \text{ m}$, $E_{\text{sys}} = 1.78 \text{ kJ}$.

The basin of attraction of y^* defines how robust the system is against disturbances in initial conditions. To enlarge this basin of attraction, Seyfarth and Geyer (2002) used the influence of the parameter α on the shape of the return map. For any given initial height y_i , they adapted α such that the corresponding return map projects into a desired height $y_{i+1} = y_{\text{des}}$ within one step (note that y_{des} is given with respect to the ground level of step i and not to a global level), generating a deadbeat control $\alpha(y_i)$ (figure 2). Although this control can be embedded as a feedback control which continuously measures the distance to the ground after the apex event, the authors used the coupling between falling time and ground distance

$$t_{\text{fall}} = \sqrt{\frac{2}{g}[y - \ell_0 \sin(\alpha)]} \quad (2)$$

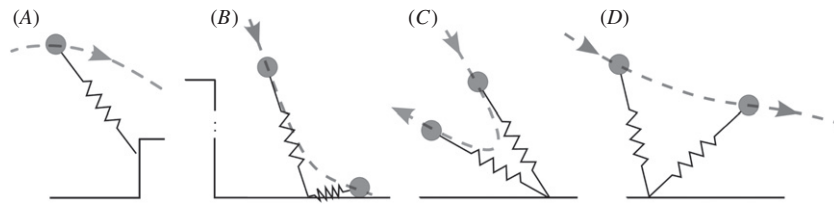


Figure 3. Failure conditions. (A) The upward step is too high giving an example of the stumbling edge (A_1 in figure 2 and A in figure 4). (B) The downward step is too large demonstrating the collision edge (B in figure 4). (C) If the spring is too stiff or the leg orientation is too flat, the model reverses direction. (D) If the spring is too soft or the leg orientation too steep the model overruns a step (A_2 in figure 2).

to derive a feedforward control $\alpha(t)$ that enforces the deadbeat behavior without having to measure the actual ground distance.

The self-stability control $\alpha(t)$ introduced by Seyfarth and Geyer (2002) largely increases the basin of attraction for steady-state solutions in spring-mass running. But it also has limitations. First, the tolerated upward steps in locomotion are restricted by the landing condition (1), see also figure 3(A). For self-stability control the maximum tolerance for upward steps is

$$y_{\max, \text{up}} = y_{\text{des}} - \ell_0 \sin(\alpha_{\min}), \quad (3)$$

where α_{\min} is given by the dynamics of the system and depends on the desired apex height y_{des} , as well as the model parameters. For instance, to generate deadbeat behavior ($y_{i+1} = y_{\text{des}}$) in human-like running with parameters $y_{\text{des}} = 1$ m, $k = 30$ kN m⁻¹, $\ell_0 = 1$ m, and $E_{\text{sys}} = 1.78$ kJ (corresponding to a horizontal speed of 5 m s⁻¹, an apex height $y_i = 1$ m which equals the rest leg length ℓ_0 and a body weight of $m = 80$ kg; for typical parameters see Arampatzis et al (1999), Seyfarth et al (2002), Grimmer et al (2008)), a minimum leg orientation $\alpha_{\min} = 68.15$ deg is required, and upward steps of only 7 cm are tolerated (left gray arrow in figure 2). In contrast, downward steps show a much larger tolerance, dominated by the spring stiffness k . If the spring is too soft, the center of mass crashes into the ground during stance (figure 3(B)). An upper bound for the maximum tolerance is given by

$$y_{\max, \text{dn}} = \frac{k/2 \cdot \ell_0^2 - E_{\text{sys}}}{mg} \quad (4)$$

corresponding to the energy $E_{\text{sys}} + E_{\text{dn}}$ that can be stored in the fully compressed spring, where $E_{\text{dn}} = y_{\max, \text{dn}} \cdot mg$ is the potential energy of the maximum downward step $y_{\max, \text{dn}}$. For the same human-like parameters, this analytically estimated tolerance amounts to 16.84 m (in simulation we confirmed this approximated limit by finding solutions with 16.8 m drops and $\alpha_{\text{TD}} = 74.85$ deg). Although it is an unrealistic scenario for human running, it indicates that downward steps are uncritical if the leg stiffness and orientation is chosen properly (see also large y_i and corresponding range of α for a successful contact in figure 2). A mismatch of these two parameters not only can result in a crash but also in a reverse of direction (α exceeding the upper boundary C in figure 2, figure 3(C)) or to overrunning steps (α exceeding A_2 in figure 2, figure 3(D)) for steps down as well as for steps up.

Nevertheless, the tolerance to an upward step largely limits the robustness of spring-mass running. This critical limitation becomes even more apparent if, instead of a single

Table 1. Numerical parameters of the simulations.

Parameter	Value	Examples in
g	9.81 m s ⁻²	General
m	80 kg	
ℓ_0	1 m	
y_{des}	1 m	General, except figures 6 and 8
E_{sys}	1.78 kJ	General, except section 3.2, figures 6 and 8
k	30 kN m ⁻¹	Section 2
α	$\alpha = \alpha(t_{\text{fall}})$	
k	$k = k(t_{\text{fall}})$	Sections 3 and 4
α	$\alpha = \alpha(t_{\text{fall}})$	
E_{sys}	$E_{\text{sys}} = E_{\text{sys}}(v_x, y, \Delta y)$	Section 3.2

step, the average change in ground level over many steps is considered. Because the step tolerance is limited to 7 cm in the upward direction, average changes in ground level of only about $y_{\text{tol}} = \pm 3.5$ cm are guaranteed to be tolerated when running over rough terrain in which up and down steps vary randomly (this human-like self-stability control is referred to as *self-stability control* in the remainder of this paper). Even if the stiffness is optimized to increase y_{tol} ($k_{\text{opt}} \approx 7$ kN m⁻¹), the maximum guaranteed tolerance does not exceed ± 9 cm (compare table 2).

Another limitation of the self-stability control computed by Seyfarth and Geyer (2002) is that it does not take into account changes in system energy introduced by changing ground levels from step to step. The self-stability control is computed for a fixed system energy E_{sys} . However, with changing ground levels from step to step, the system energy changes as well, and the deadbeat behavior gets imprecise (what in general decreases the guaranteed tolerance, $y_{\text{tol}} < 1/2 \min(y_{\max, \text{dn}}, y_{\max, \text{up}})$). Although the authors found that the control is quite robust against such changes in E_{sys} , it is strictly valid only for $\Delta E_{\text{sys}}/E_{\text{sys}} \ll 1$.

3. Extending self-stability control

In this section we expand the theoretical limits of self-stability control. We largely improve its tolerance against ground disturbances (tenfold in our human-like example), and precision its enforcement of deadbeat behavior. We achieve the first by introducing another parameter variation in flight besides the leg orientation $\alpha(t)$, and the second by incorporating changes in system energy into the return map analysis.

Table 2. Tolerances to ground level changes (for a single step up $y_{\max,\text{up}}$ or down $y_{\max,\text{dn}}$ and random changes y_{tol}) for the different controls presented in this study (desired apex height $y_{\text{des}} = 1\text{ m}$, apex height $y_i = 1\text{ m}$ and velocity $v_{x,i} = 5\text{ m s}^{-1}$ at start corresponding to a system energy $E_{\text{sys}} = 1.78\text{ kJ}$). The indices (A, B, C, D) on the single step tolerances refer to the cause of failure when exceeding it, see figure 3.

Control	$y_{\max,\text{up}}$ and $y_{\max,\text{dn}}$	y_{tol}	Notes
Self-stability controls $\alpha(t_{\text{fall}})$ (Seyfarth <i>et al</i> 2002), examples section 2			
Human example	7 cm ^A and > 1 m ^C	3.5 cm	Fixed k ($k = 30\text{ kN m}^{-1}$)
k_{opt} example ^a	33 cm ^A and 53 cm ^D /> 1 m ^E	9 cm	Fixed and optimized k ($k = 7\text{ kN m}^{-1}$); exceed limits ($\mu, \Delta\ell$) of section 4
Extended self-stability controls $[\alpha, k](t_{\text{fall}})$, examples sections 3 and 4			
$[\alpha, k]_{\text{bal}}(y_i = 1\text{ m})$			
Balanced control	32 cm ^A and 32 cm ^C	0 cm	Fixed $[\alpha, k]$; unstable fixed point
$[\alpha, k]_{\text{bal}}(t_{\text{fall}})$			
Balanced control	33 cm ^C and 47 cm ^D /> 1 m ^E	10 cm	Exceed limits ($\mu, \Delta\ell$) of section 4
$[\alpha, k]_{\text{stiff}}(t_{\text{fall}})$			
Stiff control	70 cm ^C and 67 cm ^D /> 1 m ^E	32 cm	$k_{\text{max}} = 50\text{ kN m}^{-1}$; exceed limits (t_c, GRF)
Stiff control ^b	77 cm ^A and $\gg 1\text{ m}^B$	33 cm	$k_{\text{max}} = 50\text{ kN m}^{-1}$; exceed limits (t_c, GRF)
Stiff control	29 cm ^A and 49 cm ^D /> 1 m ^E	13 cm	Include limits of section 4
Extended stability controls $[\alpha, k](t_{\text{fall}})$ with v_x feedback			
Control example ^c	77 cm ^A and $\gg 1\text{ m}^B$	37 cm	$k_{\text{max}} = 50\text{ kN m}^{-1}$; for different strategies (e.g. soft or stiff)

^a Fixed stiffness—optimized control with respect to y_{tol} , see section 2.

^b Control estimated with one $E_{\text{sys}} \neq \text{const.}$ hypersurface ($v_x = 5\text{ m s}^{-1}$), see section 3.2.

^c Controls estimated with different $E_{\text{sys}} \neq \text{const.}$ hypersurfaces, example of section 3.2.

3.1. Stiffness adaptation $k = k(t)$

Equations (3) and (4) show that the tolerance against ground disturbances depends on the parameters $y_{\text{des}}, \ell_0, m, g,$ and k (note that α_{min} in (3) itself depends on y_{des}, k and E_{sys}). While E_{sys}, m and g are constant system parameters, and y_{des} is a given target value, the leg parameters k and ℓ_0 can be accessed in addition to $\alpha(t)$ to manipulate the return map of spring-mass running during flight. The influence of these two parameters is not equal, however. Whereas changes in k and ℓ_0 shape the system dynamics, changes in ℓ_0 also affect leg geometry. Because it is subject to additional technical limitations (compare section 4), we avoid changing leg geometry, and focus on the spring stiffness k as the parameter for influencing the return map. Such a variation in k before touchdown (TD) can be achieved in robots, for instance, by using actuators in series or parallel with the leg spring (Raibert 1986, Hosoda *et al* 2008, Hurst and Rizzi 2008, Vanderborght *et al* 2009), and in humans by the level of the pre-activation of antagonistic muscle groups (Hortobágyi and DeVita 2000, Müller *et al* 2010).

Allowing k to adapt in flight in addition to α , we obtain by brute-force mapping many pairs $[\alpha, k](y_i, y_{\text{des}})$ that project from an initial apex height y_i to a desired height y_{des} in spring-mass running. Figure 4 shows these many solutions as a hypersurface S_y in the parameter space $[k, \alpha, y_i]$ for the same desired height $y_{\text{des}} = 1\text{ m}$ and human-like system parameters $E_{\text{sys}}, \ell_0, m$ and g as in the example of section 2. The yellow line in S_y marks the deadbeat control

$\alpha(y_i)$ shown in figure 2 for the constant spring stiffness $k = 30\text{ kN m}^{-1}$. The borders A and C again mark the upward stumbling border, corresponding to the landing condition (1), and the energy limit $y = E_{\text{sys}}/mg$, respectively. The dashed line shows the parameter combinations that correspond to start heights $y_i = y_{\text{des}}$. The intersection of this line with the yellow solid line identifies the parameter α that corresponds to the fixed point solution $y_i = y_{i+1}$. Another border of S_y occurs for low stiffness values. At this border B the leg is too soft and the system crashes during stance (figure 3(B)). Thus, B is related to the tolerance against downward steps.

A and B help to understand strategies and constraints for changing k and α in flight to maximize tolerances against ground disturbances. Consider the parameter combinations that belong to the apex height $y_i = y_{\text{des}}$ shown by the dashed line in figure 4. The maximum tolerance against upward steps (3) is obtained for the smallest possible α corresponding to the left edge of this line. At this edge, however, the tolerance against downward steps is near zero as k approaches $k_{\text{min}} = 2E_{\text{sys}}/\ell_0^2$, which describes zero tolerance against downward steps (4). Moving along the dashed line toward large k , the stiffness $k(\alpha, y_i)$ that produces equal tolerances for up and down steps ($y_{\max,\text{up}} = y_{\max,\text{dn}}$) can be estimated by equating and rewriting (3) and (4) ($y_{\text{des}} - \ell_0 \sin(\alpha_{\text{min}}) = (k/2 \cdot \ell_0^2 - E_{\text{sys}})/mg$) with $y_{\text{des}} = y_i$ to

$$k(\alpha, y_i) = \frac{2}{\ell_0^2} \{ [y_i - \ell_0 \sin(\alpha)] mg + E_{\text{sys}} \}. \quad (5)$$

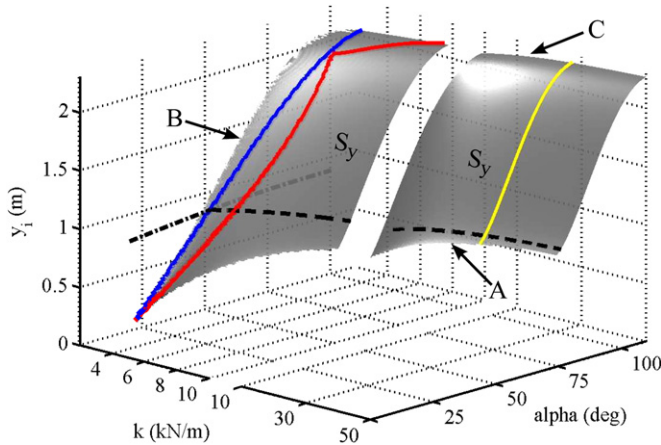


Figure 4. Parameter combinations enforcing deadbeat control. The hypersurface S_y (gray) shows all parameter combinations $[k, \alpha](y_i)$ that enforce $y_{i+1}(y_i) = y_{des}$ with $y_{des} = 1$ m. The edges of the surface describe the stumbling edge (A), the collision edge for which the mass collides with the ground during spring compression (B), and the energy limit $y_i mg = E_{sys}$ (C) (S_y is not limited for increasing k). The yellow, blue and red lines (right/light gray, left/dark gray and middle/gray lines, respectively) show alternative deadbeat control strategies $[k, \alpha](y_i)$, including the previous deadbeat control $\alpha(y_i)$ (compare section 2 and figure 2) (yellow/light gray), and the *balanced control* as approximated by equation (5) (blue/dark gray) and as computed numerically (red/gray). The dashed black curve indicates fix-point solutions $y_i = y_{i+1} = y_{des}$ and the dashed-dotted curve shows the relation $k(\alpha, y_i = y_{des})$ of the *balanced control* approximation (5). Note that for large y_i the red and blue controls merge at one point when the spring fully compresses. Above this point the tolerance to downward steps (y_{dn}) is limited by the constraint $y(t_{TO}) > y(t > t_{TO})$ (figure 3(D), A_2 in figure 2), and below this point, by backward movement ($v_{x,i+1} < 0$, figure 3(C)) (rather than by the full compression constraint (4)).

A balanced, maximized tolerance in both directions $y_{max,dn}(y_i) = y_{max,up}(y_i)$ is achieved when this $k(\alpha, y_i)$ relationship intersects the dashed line $y_i = y_{des}$. This estimated parameter combination $[k, \alpha]_{bal}(y_i)$ is depicted in figure 4 as a blue line for all possible initial heights y_i along with its computed and more exact counterpart (red line, referred to as *balanced control* in the remainder of this paper).

If the spring-mass model can adjust its parameters to the measured ground level only once at apex, the choice $[k, \alpha]_{bal}(y_i)$ will maximize the tolerance against unexpected disturbances in ground level after the apex event. For instance, for the desired apex height $y_{des} = 1$ m and for starting in steady-state, the *balanced control* tolerance $y_{dn}(y_i) = y_{up}(y_i)$ is about 32 cm for one step (as compared to only 7 cm for the deadbeat control $\alpha(t)$, compare section 2 and table 2). Larger tolerances can be achieved if the parameters k and α can be continuously adapted after the apex event within the surface S_y to apex heights \hat{y}_i that correspond to the altered ground level. If this ground level needs to be continuously sensed for adaptation, $[k, \alpha]_{bal}(\hat{y}_i)$ maximizes the tolerance against sensor noise.

Because apex height y_i and falling time t_{fall} after apex are uniquely coupled (2), the ground level does not need to be measured for continuous adaptation, and many alternative control strategies for k and α exist. Figure 5 shows the transformed hypersurface $S_y \rightarrow S_t$ in the $[k, \alpha, t_{fall}]$ space.

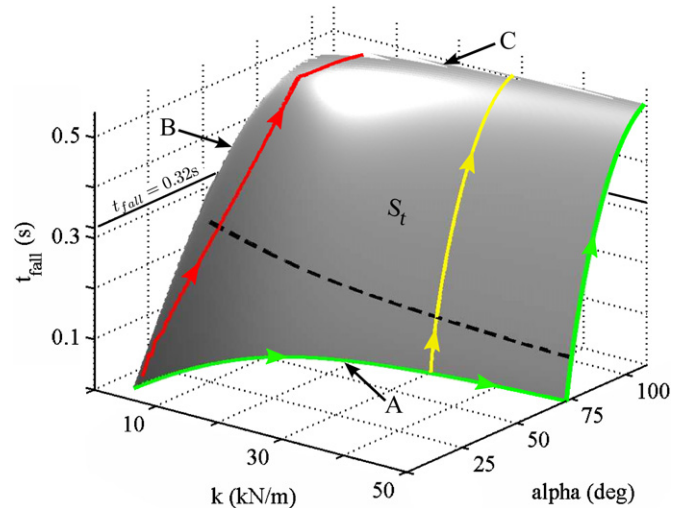


Figure 5. Parameter combinations for extended self-stability controls. The hypersurface S_t shows all time-transformed parameter combinations $[k, \alpha](t_{fall})$ for $y_{des} = 1$ m. The borders A, B, C correspond to the same borders of S_y (figure 4). The yellow, red and green curves (center/light gray, left/gray and bottom-right/light gray curves on the hypersurface, respectively) show the time evolutions of the *self-stability control* $\alpha(t_{fall})$, the calculated *balanced control* $[k, \alpha]_{bal}(t_{fall})$, and the *stiff control* $[k, \alpha]_{stiff}(t_{fall})$, respectively. The dashed curve indicates parameter combinations for the fixed point solutions $y_i = y_{i+1} = y_{des}$. The black line on $t_{fall} = 0.32$ s indicates the slice plane used in figures 6(A) and (C).

As long as parameter combinations $[k, \alpha]$ evolve in time t_{fall} on S_t (indicated by the arrows for depicted controls), y_{des} will for $\Delta E_{sys} \ll E_{sys}$ (compare section 2) be reached in the next apex independent of the actual change in ground level that the model experiences during the step. For example, the yellow solid line evolution shows the *self-stability control* $\alpha(t)$, which is the transformed deadbeat control $\alpha(y_i)$ for $k = 30$ kN m⁻¹. Figure 5 also shows the *balanced control* that remains close to the border B (red line). A third example is a ‘stiff’ control that follows the border A nearly instantaneously, and then evolves on the surface for $k = 50$ kN m⁻¹ (referred to as *stiff control* in the remainder of this paper). If the system energy E_{sys} is not adapted from step to step to accommodate changes in potential energy due to ground level changes in previous steps, these three control alternatives show different, guaranteed ground tolerances y_{tol} in locomotion, ranging from 3.5 cm for the *self-stability control* (section 2), to 10 cm for the *balanced control*, and to 32 cm for the *stiff control* (see table 2). (If k increases further, for the *stiff control* the guaranteed tolerance approaches the numerically estimated limit of about 40 cm given by $\alpha_{min} = 10.6$ deg, (3).)

3.2. Energy variations

The performance of the different control strategies differs only because E_{sys} is assumed to be constant. Figure 6 shows as contour plots for two different falling times (panels (B) and (C)) the parameter combinations α and k which correspond for a constant system E_{sys} to different desired apex heights. The parameter combinations for $y_{des} = 1$ m are highlighted as a white solid line. In both panels (B) and (C), neighboring

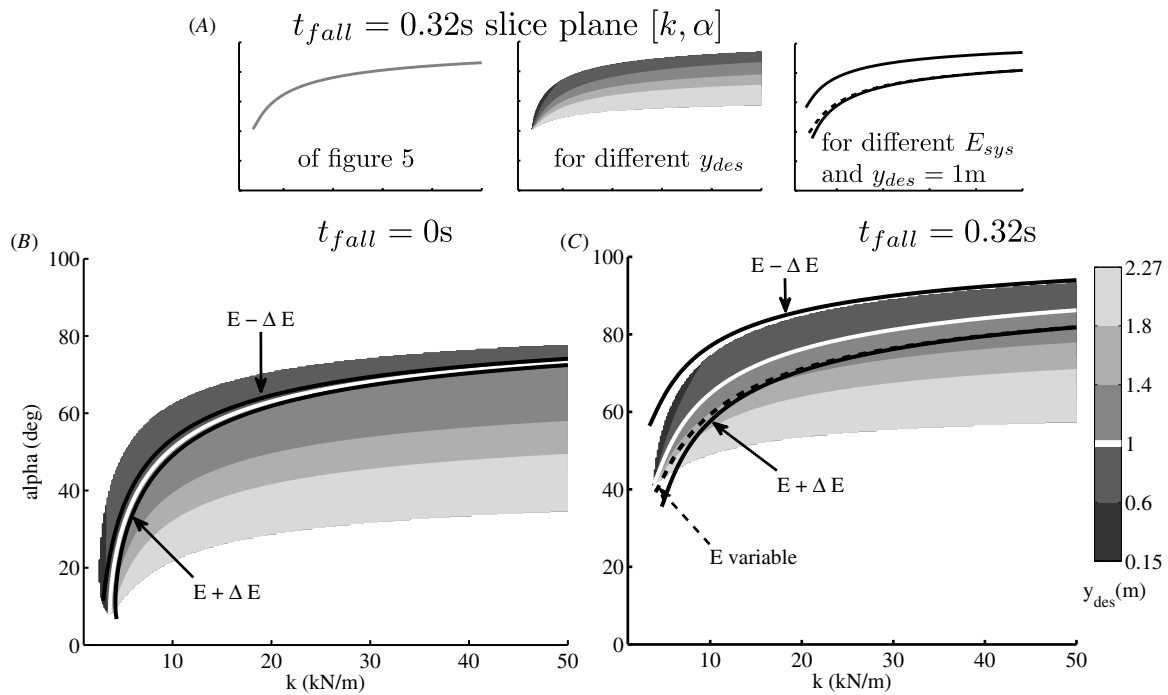


Figure 6. Influence of system energy E_{sys} on the desired apex height y_{des} and corresponding parameter combinations $[k, \alpha]$ for two different falling times, $t_{\text{fall}} = 0\text{ s}$ (B, falling height $\Delta y = 0\text{ m}$) and $t_{\text{fall}} = 0.32\text{ s}$ (A and C, falling height $\Delta y = 0.5\text{ m}$). (A) The panels describe qualitatively how the slice plane $t_{\text{fall}} = 0.32\text{ s}$ of figure 5 changes for different y_{des} and for different E_{sys} . (B) and (C) For the two different falling times the white curve (gray in A) shows $[k, \alpha]$ combinations for $y_{\text{des}} = 1\text{ m}$. The contour plots show the parameter combinations for different desired apex heights y_{des} ranging from 0.15 to 2.27 m. The black solid curves show $[k, \alpha]$ combinations for the same $y_{\text{des}} = 1\text{ m}$ but modified system energies $E \pm \Delta E$, equivalent to encountered steps of $\Delta y = 0.5\text{ m}$. The dashed curve indicates parameter configurations leading to $y_{\text{des}} = 1\text{ m}$ if the system energy is adapted to account for up and down steps (only shown in A and C).

solutions $y_{\text{des}} = 1\text{ m} \pm \Delta$ are farther apart for large α and k than for small ones, showing that the tolerance against parameter errors increases with increased parameter values, independent of the falling time. For comparison, the same parameter relationship for $y_{\text{des}} = 1\text{ m}$ is shown as black solid lines for changed system energies $E_{\text{sys}} \pm \Delta E$ equivalent to encountered steps of $\Delta y = \pm 50\text{ cm}$. While these relationships lie close to the same relationship for E_{sys} initially (panel (B)), they clearly drift apart with increasing falling time (panel (C)), showing that errors in estimating E_{sys} are tolerated more for short falling times than for long ones. As a consequence, controls that are developed assuming a constant system energy will tolerate large steps if they approach large values of α and k in the shortest time possible. Thus, of the two controls derived in the previous section, the *stiff control* performs better than the *balanced control* ($y_{\text{tol}} = 32\text{ cm}$ versus 10 cm , respectively).

In self-stability controls the assumed constant E_{sys} including inherent errors in the parameter adjustment not only influence the guaranteed tolerances to multiple random changes in the ground level y_{tol} within the different controls but also the tolerance to single step perturbations $y_{\text{max,up}}$ and $y_{\text{max,dn}}$. Table 2 shows these estimated tolerances and the causes of failure. For example, the limiting factor for steps up in the *stiff control* ($y_{\text{max,up}} = 70\text{ cm}$) and the *balanced control* ($y_{\text{max,up}} = 33\text{ cm}$) is not the stumbling edge but the reverse in direction (compare figures 3(A) and (C)). As a result of the error propagation over many perturbed steps y_{tol} is in general less than half of the limiting step, e.g. for the *balanced control* is $y_{\text{tol}} < 1/3 y_{\text{max,up}}$.

The different performances can be equalized and maximized by including in the derivation of the control strategies the energy fluctuations $\Delta E = mg\Delta y$ that occur from step to step due to changes in potential energy. We achieve this by computing the apex return map $y_{i+1} = R(y_i)$ for different y_i without adapting the initial forward speed $v_{x,i}$ to a constant system energy E_{sys} (similar to Ernst et al (2009)) (figure 1). As a result, the *balanced* and *stiff control* strategies, which start with the minimum possible angle α_{min} , now achieve the same, improved guaranteed tolerance of about 37 cm (apart from small deviations between the strategies due to limited numerical accuracy; note also that with this method first the single step tolerances can be maximized (table 2, stiff control^b) and second the guaranteed tolerance (table 2, control example^c)). However, including the energy variation requires to adapt the return map $R(y_i)$ and therefore the control $[k, \alpha](t_{\text{fall}})$ from step to step to altered system energies. This can be achieved for instance, through an additional feedback of the horizontal velocity v_x at apex or of the value of the previous contact time t_c (Raibert 1986, Hutter et al 2010). Thus, although including an energy control improves the guaranteed tolerance, it cannot be formulated as a pure self-stability control. A self-stability control only requires a feedback of discrete bits triggering an event (in our case the reset of the leg parameters in the apex event) and does not need continuous or discontinuous feedback about the amount of the system energy or the ground level error (Ringrose 1997, Grimmer et al 2008).

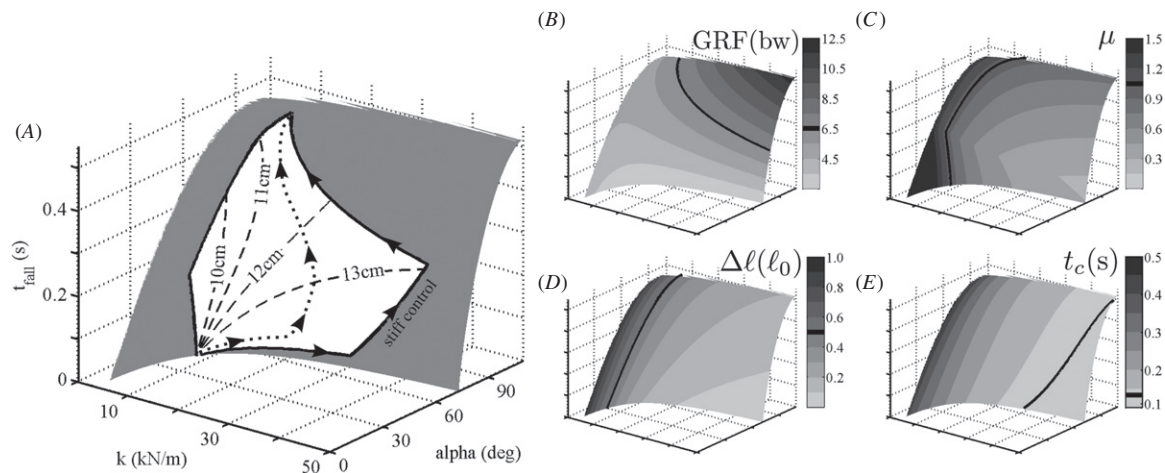


Figure 7. Influence of technical limitations on self-stability control. Panels (A)–(E) show the hypersurface S_t for $y_{des} = 1\text{m}$. The small panels (B)–(E) depict the resulting peak ground reaction force GRF (B), peak friction coefficient μ (C), peak leg compression $\Delta\ell$ (D), and ground contact time t_c (E). The solid curves in the small panels correspond to specific values for these technical limitations (GRF = 6.5 bw, $\mu = 1$, $\Delta\ell = 0.5\ell_0$, $t_c = 125\text{ms}$). Panel (A) shows how the technical limitations constrain the available parameter combinations $[k, \alpha, t_{fall}]$ for self-stability control (note that the limitation of the maximum angular velocity $\omega_{max} = 900\text{deg s}^{-1}$ is included as the lower border of the available range). Different time evolutions of $[k, \alpha]$ within the available range (white area) result in different guaranteed tolerances y_{tol} ranging from 9 to 13 cm (dashed curves). The dotted curve indicates a self-stability control that maximizes the distance to the borders of the available parameter range, resulting in the largest, combined tolerance against ground level and parameter mismatches.

4. Incorporating technical limitations in defining the control strategy

So far we have concentrated on the theoretical extensions of the self-stability control leading to substantially improved tolerances against ground disturbances. The practical use of these extensions is constrained by technical limitations and we show how incorporating these limitations distinguishes particular control strategies. For this part, we focus on pure self-stability controls that do not require feedback.

Several major technical limitations of self-stability controls exist. One is the dynamics of real actuators. The maximum angular velocity $\dot{\alpha}_{max}(t) = \omega_{max}(t)$ cannot exceed the speed limits of the hip actuators. In addition, leg actuators can only generate ranges of stiffness k due to constraints imposed by maximum torque production (maximum stiffness), reflected inertia (minimum stiffness), and maximum torque-speed relationship (maximum stiffness). Mechanical design imposes further limitations, for instance, on the allowable ground-reaction force GRF_{max} to prevent damage, on the available maximum leg compression $\Delta\ell_{max}$, and on the maximum lift $\alpha_{apex,min}$ of the leg in swing. Finally, robots do not have feet hinged to the ground as the spring mass model does, and a secure foothold requires the horizontal GRF to lie within the friction cone, $\text{GRF}_x < \mu \cdot \text{GRF}_y$.

We map these limitations onto five parameters and demonstrate with an example how they influence the identification of self-stability controls. Besides a friction coefficient $\mu = 1$, the dynamic parameters include a maximum angular velocity $\omega_{max} = 900\text{deg s}^{-1}$ and a minimum contact time $t_{c,min} = 125\text{ms}$. Rather than a stiffness limit, the one on the contact time eases the comparison to technical actuators. Combined with the mechanical parameters of an assumed

maximum ground reaction force, $\text{GRF}_{max} = 6.5$ body weights, and a maximum leg compression, $\Delta\ell_{max} = 0.5\ell_0$, it translates into a torque-speed relationship for electrical actuators. (We do not limit the minimum leg angle α_{min} in our example, because it will be automatically constrained by μ_{max} and $\Delta\ell_{max}$.) The parameter values do not describe a specific human or robot. They represent reasonable estimates motivated by literature (e.g. (Miller and Nissinen 1987, Minetti et al 1998)). Note that the described method of customizing the self-stability control is independent of these specific values.

Figure 7 shows how the technical limitations constrain the parameter choices in the hypersurface S_t for self-stability control. Panels (B)–(E) show the individual trends of GRF, μ , $\Delta\ell$, and t_c . The peak ground reaction force increases from low to high stiffness values and with rising falling times (figure 7(B)). The ratio $\text{GRF}_x/\text{GRF}_y$ decreases from flat to steep angles of attack, but shows a trend reversal in the time evolution (figure 7(C)). The trend reversal occurs at falling times that result in steady-state stance phases with symmetric GRF patterns (take-off angle equals TD angle). For shorter falling times, the model hits with flatter angles and $\text{GRF}_x/\text{GRF}_y$ increases. For larger falling times, it pushes off with flatter angles and a similar increase in $\text{GRF}_x/\text{GRF}_y$ occurs. Finally, the maximum leg compression and contact time show similar behaviors decreasing from low to high stiffness values and from flat to steep angles of attack (figures 7(D) and (E)). The example limitations are plotted as lines in the individual panels (figures 7(B)–(E)), restricting the available combinations of k and α for self-stability control in S_t (figure 7(A)).

Although the parameter combinations available for self-stability control are reduced, a substantial variety remains (figure 7(A)). In general, the static friction μ (as in our

example) and the maximum leg compression $\Delta\ell_{\max}$ shift the smallest possible angle of attack toward larger values (from 10.6 deg to 45.0 deg), reducing the tolerance against upward steps for all possible control strategies. In particular, the *balanced control* introduced in section 3 cannot be followed anymore since it lies outside of the feasible parameter range. On the other hand, the minimum contact time $t_{c,\min}$ or the maximum ground reaction force (GRF_{\max}) reduce the maximum leg stiffness that can be achieved in contact (from 50 to 41 kN m^{-1} and clearly less for increasing falling times), reducing the tolerance against downward steps. Although the *stiff control* is still available, it requires to follow the borders defined by GRF_{\max} and $t_{c,\min}$ as well as by the maximum angular velocity ω_{\max} (indicated by arrows following the borders). (Note that the ω_{\max} border is not fixed but depends on the start value of α_{\min} . In the *stiff control* example, it limits how fast the leg angle can shift from the smallest possible value to the maximum value defined by the t_c border.) As a result the guaranteed tolerance reduces from 32 to 13 cm. A control that follows the parameter combinations defined by the borders, however, is at risk of exceeding the technical limits if errors in the parameter adaptation occur. In realistic situations such errors cannot be excluded. A control that maximizes the distance to these parameter borders provides a compromise, which results in robustness not only against ground level changes but also against parameter mismatches (dotted line, figure 7(A)).

5. Conclusion and discussion

Our goal was to better understand fundamental limits of self-stability control, and to use this knowledge to optimize this control method with respect to unknown and unexpected ground disturbances. Previously derived versions of self-stability control in running tolerate large unexpected downward steps (up to 35% of leg length, (Schmitt and Clark 2009)), but cannot accommodate similarly large steps in the upward direction (less than 5% of leg length, (Seyfarth *et al* 2002, Rummel and Seyfarth 2008)) unless very bouncy gaits with large apex heights are selected ((Seyfarth and Geyer 2002, Ankarali and Saranlı 2010), figure 2). By contrast, we show that self-stability control tolerates large steps in both directions if variations of leg stiffness $k(t)$ before TD are introduced in addition to changes in the leg orientation $\alpha(t)$, resulting in an increase of ground tolerance from 3.5% (to 9% for an optimized stiffness) to about 35% of leg length for our human-like example. Key to this substantial increase is that, unlike a fixed leg stiffness, the variable stiffness allows to start with flat leg orientations ($\alpha_{\min} \rightarrow 0$ deg) after the apex event, maximizing upward step tolerances (about 70% of leg length for single steps up, table 2). Such an improved ground level tolerance in running can help robots or animals to prevent falls if reliable informations about the ground level are missing e.g. while running in the dark or across meadows with high grass camouflaging drops and bumps. In addition, we also demonstrate how technical limitations can be accounted for in the derivation of self-stability control. We achieve this by generalizing the return map manipulation for deadbeat

behavior introduced in Seyfarth and Geyer (2002) to the two parameters α and k .

Flight phase controls which, besides $\alpha(t)$, adapt leg parameters before TD have been proposed in literature; however, these controls do not explore the theoretical limit of gait stability as measured by step tolerance. For instance, Blum *et al* (2007, 2010) explore simultaneous changes $p = \dot{p}_0 t + p_0$ after the apex event for the three parameters leg stiffness, orientation and length ($p = k, \alpha, \ell$). The authors demonstrate with their controls that previously unstable fixed point solutions $y_i = y_{i+1}$ can be stabilized, but they do not explore if these controls maximize the guaranteed tolerance y_{tol} . Our extended self-stability control achieves this maximization as long as the control hyper-surface $S_t(E_{\text{sys}})$ exists, distinguishing this approach from other control approaches that do not actively exploit the return map manipulation. Although we have focused in this paper on one particular example using model parameters equivalent to human running at 5 ms^{-1} with a desired apex height of 1 m, figure 8 shows that S_t exists for a large range of human running speeds and desired apex heights.

In contrast to the ideal spring-mass model, real legged systems in engineering and biology are subject to constraints on, for instance, mechanical design, actuation, and ground friction. To understand how such realistic constraints influence self-stability control, we introduced limits on model parameters and variables that reflect technical and physical limitations found in legged systems, and studied their effect on the available control solutions. Our results show that although realistic constraints reduce the parameter combinations available for self-stability control, a substantial variety remains and large tolerances can still be guaranteed (13% leg length for the limit set $\Delta\ell_{\max} = 50\%$ leg length, $\mu = 1$, $\text{GRF}_{\max} = 6.5 \text{ bw}$, $t_{c,\min} = 125 \text{ ms}$, $\omega_{\max} = 900 \text{ deg s}^{-1}$ and an apex height that equals the leg length, figure 7(A)). More generally, we find that embedding and interpreting technical limitations within the surface $S_t(E_{\text{sys}})$ provides a design method to customize self-stability control for individual legged systems.

Besides technical limitations, losses in energy and their compensation form an integral part of locomotion systems which are not captured by the conservative spring-mass model. In deriving the control surface S_t , we included energy variations that occur from step to step due to changes in ground level (figure 6). We found that incorporating step-to-step adaptations $S_t \rightarrow S_t(E_{\text{sys}})$ equalizes the guaranteed tolerance for all control strategies within the surface $S_t(E_{\text{sys}})$ that start from the same angle α_{\min} , increasing the control design options. However, we required additional feedback to include the adaptation, and could not integrate it into the self-stability control. In addition, our energetically conservative model does not describe energy changes due to, for example, damping or ground friction, and their compensation. Model extensions that consider such changes have been proposed in literature (Geyer *et al* 2003, Schmitt and Clark 2009, Ankarali and Saranlı 2010, Koepl *et al* 2010) and were recently applied to a one-legged planar hopper (Andrews *et al* 2011). If the resulting Poincaré maps are unique, these extensions could

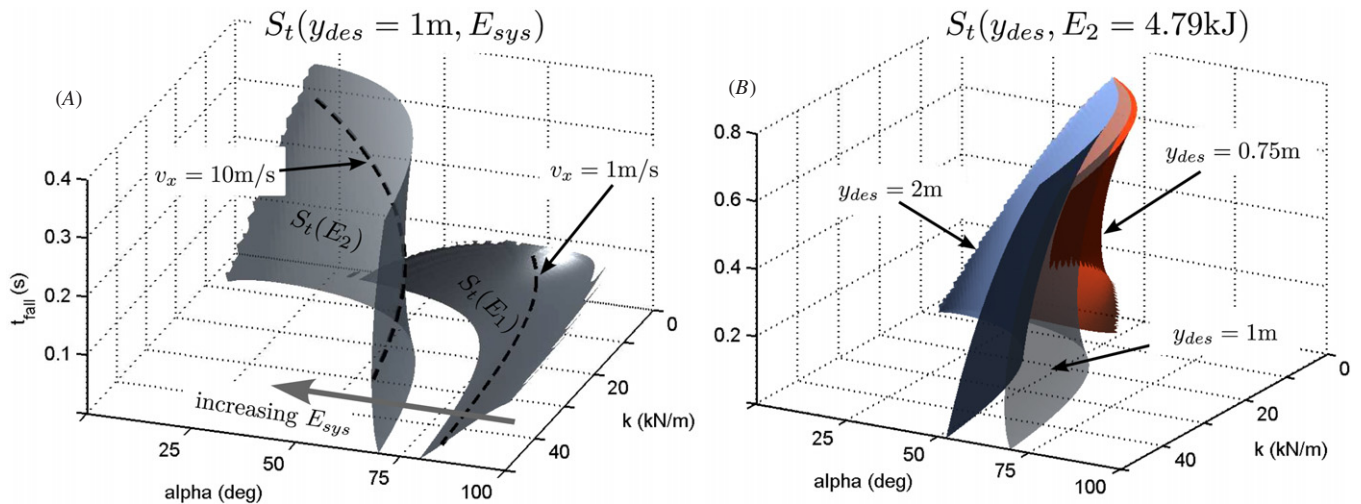


Figure 8. Existence of the hypersurface S_t for a large range of system energies E_{sys} and desired apex heights y_{des} . Panel (A) shows S_t for one apex height $y_{des} = 1\text{ m}$ at two different system energies $E_1 = 0.83\text{ kJ}$ and $E_2 = 4.79\text{ kJ}$. In steady-state running with $y_i = y_{i+1} = y_{des}$, the two energies correspond to forward speeds of 1 and 10 m s^{-1} , respectively. The dashed curves show the parameter combinations that describe these solutions. Panel (B) shows S_t for the same system energy $E_2 = 4.79\text{ kJ}$ and three different desired heights.

provide powerful tools for incorporating energy losses and their compensation in self-stability control.

While stability is of major concern to legged systems, other criteria such as energetic efficiency or comfort likely shape locomotion control in predictable environments. Humans and other animal bipeds adapt their leg parameters in running when they encounter compliant surfaces (Ferris *et al* 1998, 1999, Kerdok *et al* 2002), or expected (Grimmer *et al* 2008, Müller and Blickhan 2010) and unexpected disturbances (Daley and Biewener 2006, Daley *et al* 2007). In part this adaptation seems related to self-stability control. For instance, Daley and Biewener (2006) and Daley *et al* (2007) found that running birds retract their legs before TD, and maintain this retraction control $\alpha(t)$ even after they encounter large unexpected drops in ground level. In addition, they found that running birds change the leg length during flight, $\ell_0 = \ell_0(t)$, which correlated with net energy changes after the disturbance, indicating a feedforward contribution to energy control. On the other hand, in predictable environments such as urban walkways humans tend to minimize foot clearance. For instance, in walking, the foot ground clearance at mid-swing reaches not more than about 1 cm (Winter 1992). While this lack of lifting the leg improves energy efficiency, it substantially increases the risk of tripping (section 2), and thus requires reliable estimates about ground elevation. Similar estimates are required for ground speed matching at TD (Herr and McMahon 2001, Blum *et al* 2010), which improves energy efficiency by reducing impacts. If such estimates are available, using for instance visual feedback, energy efficiency likely subordinates ground tolerance as locomotion criterion. Another criterion could be locomotion comfort. It has been observed that, for unexpected changes in ground stiffness as well as anticipated changes in ground level, humans maintain a smooth center of mass trajectory similar to undisturbed running, independent of the actual ground stiffness (Ferris *et al* 1999, 1998) or ground level (Grimmer *et al* 2008, Ernst *et al* 2009).

Whether or not humans and animals use a feedforward control strategy, they adapt their leg parameters to the terrain in locomotion. Here we showed that the simultaneous adaptation of these parameters before TD is key to robust locomotion with largely increased tolerances to ground disturbances. In addition, we demonstrated that a substantial part of this adaptation can be embedded in feedforward, extended self-stability control, taking advantage of the relationship between ground distance and falling time in flight. And finally, we found that the flexibility of extended self-stability control allows to customize it for individual legged systems with defined technical and physical constraints.

Acknowledgments

The authors would like to thank the German Research Foundation (DFG) (ME and RB—B1236/15 and B1236/21) and the US National Science Foundation (NSF) (HG—Dynamical Systems Program, award number CMMI-1100232) for supporting this work.

References

- Alexander R M 1990 Three uses for springs in legged locomotion *Int. J. Robot. Res.* **9** 53–61
- Altendorfer R, Moore N, Komsuoglu H, Buehler M, Brown H B, McMordie D, Saranli U, Full R and Koditschek D E 2001 Rhex: a biologically inspired hexapod runner *Auton. Robots* **11** 207–13
- Andrews B, Miller B, Schmitt J and Clark J E 2011 Running over unknown rough terrain with a one-legged planar robot *Bioinspir. Biomim.* **6** 026009
- Ankarali M M and Saranli U 2010 Stride-to-stride energy regulation for robust self-stability of a torque-actuated dissipative spring-mass hopper *Chaos* **20** 033121
- Arampatzis A, Brüggemann G-P and Metzler V 1999 The effect of speed on leg stiffness and joint kinetics in human running *J. Biomech.* **32** 1349
- Blickhan R 1989 The spring-mass model for running and hopping *J. Biomech.* **22** 1217–27

- Blum Y, Lipfert S, Rummel J and Seyfarth A 2010 Swing leg control in human running *Bioinspir. Biomim.* **5** 026006
- Blum Y, Rummel J and Seyfarth A 2007 Advanced swing leg control for stable locomotion *Autonome Mobile Systeme 2007* ed W Brauer (Berlin: Springer) pp 301–7
- Collins S, Ruina A, Tedrake R and Wisse M 2005 Efficient bipedal robots based on passive-dynamic walkers *Science* **307** 1082–5
- Daley M A and Biewener A A 2006 Running over rough terrain reveals limb control for intrinsic stability *Proc. Natl Acad. Sci. USA* **103** 15681–6
- Daley M A, Felix G and Biewener A A 2007 Running stability is enhanced by a proximo-distal gradient in joint neuromechanical control *J. Exp. Biol.* **210** 383–94
- Ernst M, Geyer H and Blickhan R 2009 Spring-legged locomotion on uneven ground: a control approach to keep the running speed constant *MOBILE ROBOTICS Solutions and Challenges—Proc. of the 12th Int. Conf. on Climbing and Walking Robots* ed O Tosun, H L Akin, M O Tokhi and G S Virk (Istanbul: World Scientific) pp 639–44
- Ferris D P, Liang K and Farley C T 1999 Runners adjust leg stiffness for their first step on a new running surface *J. Biomech.* **32** 787–94
- Ferris D P, Louie M and Farley C T 1998 Running in the real world: adjusting leg stiffness for different surfaces *Proc. R. Soc. Lond. B Biol. Sci.* **265** 989–94
- Full R J and Koditschek D E 1999 Templates and anchors: neuromechanical hypotheses of legged locomotion on land *J. Exp. Biol.* **202** 3325–32
- Geyer H, Seyfarth A and Blickhan R 2003 Positive force feedback in bouncing gaits? *Proc. R. Soc. Lond. B Biol. Sci.* **270** 2173–83
- Geyer H, Seyfarth A and Blickhan R 2006 Compliant leg behaviour explains basic dynamics of walking and running *Proc. R. Soc. Lond. B Biol. Sci.* **273** 2861–7
- Grimmer S, Ernst M, Günther M and Blickhan R 2008 Running on uneven ground: leg adjustment to vertical steps and self-stability *J. Exp. Biol.* **211** 2989–3000
- Herr H M and McMahon T A 2001 A galloping horse model *Int. J. Robot. Res.* **20** 26–37
- Hortobágyi T and DeVita P 2000 Muscle pre- and coactivity during downward stepping are associated with leg stiffness in aging *J. Electromyogr. Kinesiol.* **10** 117–26
- Hosoda K, Takuma T, Nakamoto A and Hayashi S 2008 Biped robot design powered by antagonistic pneumatic actuators for multi-modal locomotion *Robot. Auton. Syst.* **56** 46–53
- Hurst J and Rizzi A 2008 Series compliance for an efficient running gait *IEEE Robot. Autom. Mag.* **15** 42–51
- Hutter M, Remy C, Hoepflinger M and Siegwart R 2010 Full state control of a slip model by touchdown detection *Proc. of the 13th Int. Conf. on Climbing and Walking Robots* pp 533–40
- Karssen J D and Wisse M 2011 Running with improved disturbance rejection by using non-linear leg springs *Int. J. Robot. Res.* **30** 1585–95
- Kerdok A E, Biewener A A, McMahon T A, Weyand P G and Herr H M 2002 Energetics and mechanics of human running on surfaces of different stiffnesses *J. Appl. Physiol.* **92** 469–78
- Koepl D, Kemper K and Hurst J 2010 Force control for spring-mass walking and running *IEEE/ASME Int. Conf. on Advanced Intelligent Mechatronics* pp 639–44
- McGeer T 1990a Passive bipedal running *Proc. R. Soc. Lond. B Biol. Sci.* **240** 107–34
- McGeer T 1990b Passive dynamic walking *Int. J. Robot. Res.* **9** 62–82
- McMahon T A 1985 The role of compliance in mammalian running gaits *J. Exp. Biol.* **115** 263–82
- McMahon T A and Cheng G C 1990 The mechanics of running: how does stiffness couple with speed? *J. Biomech.* **23** (Suppl 1) 65–78
- Miller D I and Nissinen M A 1987 Critical examination of ground reaction force in the running forward somersault *Int. J. Sport Biomech.* **3** 189–206
- Minetti A E, Ardigo L P, Susta D and Cotelli F 1998 Using leg muscles as shock absorbers: theoretical predictions and experimental results of drop landing performance *Ergonomics* **41** 1771–91
- Müller R and Blickhan R 2010 Running on uneven ground: leg adjustments to altered ground level *Hum. Mov. Sci.* **29** 578–89
- Müller R, Grimmer S and Blickhan R 2010 Running on uneven ground: leg adjustments by muscle pre-activation control *Hum. Mov. Sci.* **29** 299–310
- Owaki D and Ishiguro A 2006 Enhancing stability of a passive dynamic running biped by exploiting a nonlinear spring *IEEE/RSJ Int. Conf. on Intelligent Robots and Systems* (Beijing, China) pp 4923–8
- Owaki D, Osuka K and Ishiguro A 2009 Understanding the common principle underlying passive dynamic walking and running *IEEE/RSJ Int. Conf. on Intelligent Robots and Systems* pp 3208–13
- Papadopoulos D and Buehler M 2000 Stable running in a quadruped robot with compliant legs *Proc. IEEE Int. Conf. on Robotics and Automation* vol 1 pp 444–9
- Park H-W, Sreenath K, Hurst J and Grizzle J 2011 Identification of a bipedal robot with a compliant drivetrain *IEEE Control Syst.* **31** 63–88
- Radkhah K, Lens T, Seyfarth A and von Stryk O 2010 On the influence of elastic actuation and monoarticular structures in biologically inspired bipedal robots *Proc. IEEE Int. Conf. on Biomedical Robotics and Biomechatronics* pp 389–94
- Raibert M H 1986 *Legged Robots That Balance (Artificial Intelligence Series)* (Cambridge, MA: MIT Press)
- Ringrose R 1997 Self-stabilizing running *Proc. IEEE Int. Conf. on Robotics and Automation* vol 1 pp 487–93
- Rummel J and Seyfarth A 2008 Stable running with segmented legs *Int. J. Robot. Res.* **27** 919–34
- Schmitt J 2006 A simple stabilizing control for sagittal plane locomotion *J. Comput. Nonlinear Dyn.* **1** 348–57
- Schmitt J and Clark J 2009 Modeling posture-dependent leg actuation in sagittal plane locomotion *Bioinspir. Biomim.* **4** 46005
- Schmitt J and Holmes P 2000a Mechanical models for insect locomotion: dynamics and stability in the horizontal plane I. Theory *Biol. Cybern.* **83** 501–15
- Schmitt J and Holmes P 2000b Mechanical models for insect locomotion: dynamics and stability in the horizontal plane-II. Application *Biol. Cybern.* **83** 517–27
- Seipel J and Holmes P 2007 A simple model for clock-actuated legged locomotion *Regular Chaotic Dyn.* **12** 502–20
- Seipel J E, Holmes P J and Full R J 2004 Dynamics and stability of insect locomotion: a hexapedal model for horizontal plane motions *Biol. Cybern.* **91** 76–90
- Seyfarth A and Geyer H 2002 Natural control of spring-like running—optimized self-stabilization *Proc. of the 5th Int. Conf. on Climbing and Walking Robots* ed P Bidaud and F B Amar (Bury St. Edmunds and London, UK: Professional Engineering Publishing Limited) pp 81–85
- Seyfarth A, Geyer H, Günther M and Blickhan R 2002 A movement criterion for running *J. Biomech.* **35** 649–55
- Sugimoto Y and Osuka K 2005 Stability analysis of passive-dynamic-walking focusing on the inner structure of Poincare map *Proc. 12th Int. Conf. on Advanced Robotics* pp 236–41
- Vanderborght B, Van Ham R, Lefeber D, Sugar T G and Hollander K W 2009 Comparison of mechanical design and energy consumption of adaptable, passive-compliant actuators *Int. J. Robot. Res.* **28** 90–103
- Winter D A 1992 Foot trajectory in human gait: a precise and multifactorial motor control task *Phys. Ther.* **72** 45–53